In Situ Repair of High-Performance, Flexible Nanocrystal Electronics for Large-Area Fabrication and Operation in Air

Ji-Hyuk Choi,[†,⊥] Soong Ju Oh,[†] Yuming Lai,[‡] David K. Kim,[†] Tianshuo Zhao,[†] Aaron T. Fafarman,[‡] Benjamin T. Diroll,[§] Christopher B. Murray,[†,§] and Cherie R. Kagan[†,‡,§,*]

[†]Department of Materials Science and Engineering, [‡]Department of Electrical and Systems Engineering, and [§]Department of Chemistry, University of Pennsylvania, Philadelphia, Pennsylvania 19104, United States and [⊥]Complex Assemblies of Soft Matter, CNRS-Rhodia-UPenn UMI 3254, Bristol, Pennsylvania 19007, United States

ABSTRACT

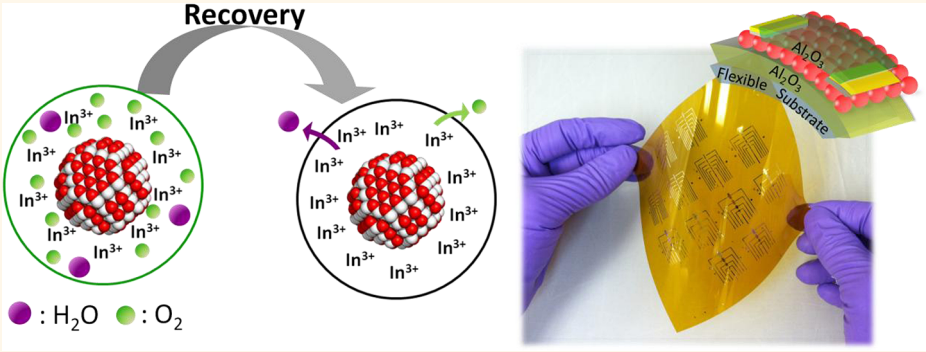

Colloidal semiconductor nanocrystal (NC) thin films have been integrated in light-emitting diodes, solar cells, field-effect transistors (FETs), and flexible, electronic circuits. However, NC devices are typically fabricated and operated in an inert environment since the reactive surface and high surface-to-volume ratio of NC materials render them sensitive to oxygen, water, and many solvents. This sensitivity has limited device scaling and large-scale device integration achievable by conventional fabrication technologies, which generally require ambient air and wet-chemical processing. Here, we present a simple, effective route to reverse the detrimental effects of chemical and environmental exposure, by incorporating, *in situ*, a chemical agent, namely, indium metal, which is thermally triggered to diffuse and repair the damage. Taking advantage of the recovery process, CdSe NC FETs are processed in air, patterned using the solvents of lithography, and packaged by atomic layer deposition to form large-area and flexible high-performance NC devices that operate stably in air.

KEYWORDS: cadmium selenide · recovery · encapsulation · field-effect transistor · flexible electronics · nanocrystal · passivation

Colloidal semiconductor nanocrystals (NCs) are attractive for their unique size-dependent electronic properties.[1,2] NCs, tailored synthetically in size, shape, and composition, have been assembled to form thin-film solids in electronic and optoelectronic solid-state devices, such as field-effect transistors (FETs),[3−6] solar cells,[7,8] light-emitting diodes (LEDs),[9,10] and complex, integrated, electronic circuits on flexible plastics.[11] Record device performances in NC FETs with mobilities >16 cm^2/Vs,[4,5,12] NC solar cells with efficiencies >7%,[13] and visible[14] and near-infrared[15] NC LEDS with radiances of ∼20 and 6.4 W/sr m^2, respectively, have been achieved. These advances have been realized through tailoring of the interparticle spacing and through doping of the NC solids, engineering charge injection and transport and radiative recombination in NC devices.

While excellent electronic and optoelectronic NC devices are being demonstrated in academic and industrial laboratories worldwide, their emergence and wide adoption commercially requires compatibility with large-area, low-cost fabrication technologies. As colloids, NCs can be processed like inks and promise low-cost, large-area solution-based coating and printing of NC devices. However, the reactive surfaces of semiconductors

* Address correspondence to kagan@seas.upenn.edu.

Received for review July 21, 2013 and accepted August 16, 2013.

Published online August 16, 2013
10.1021/nn403752d

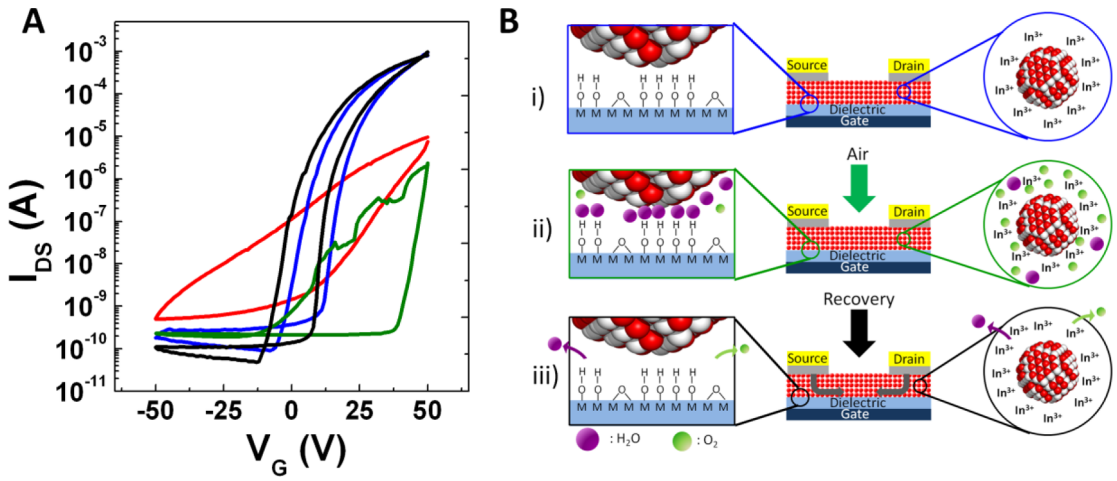

Figure 1. (A) I_D-V_G characteristics of CdSe NC thin films annealed at 250 °C for 10 min prior to In/Au electrode deposition (red) and then annealed at 250 °C for 10 min to allow indium diffusion and device doping (blue), exposed to air for 30 min (green), and reannealed at 200 °C for 5 min (black). (B) Schematic of NC FET recovery after air exposure: (i) indium-doped CdSe NC devices, (ii) exposed to air adsorb oxygen and water at the NC and gate oxide surfaces, were (iii) recovered upon annealing under nitrogen as oxygen and water desorbs and additional indium diffuses from the electrode reservoirs.

combined with the high surface-to-volume ratio of NCs cause semiconductor NCs to be sensitive to air and solvents,[16−21] typically limiting their fabrication to nitrogen gloveboxes and to dry processes. Here we introduce an *in situ* recovery agent, namely, indium metal, into the NC device and show by thermally triggering the recovery agent that the detrimental effects of air and solvent exposure are reversed. This opens up the established, expansive infrastructure and capabilities of conventional, ambient-air semiconductor fabrication technologies and the increasing number of imaginative, unconventional fabrication processes being developed for the large-area integration and production of solution-processable NC materials and device applications. Here, we exemplify the advantage of the recovery process by integrating conventional photolithography and atomic layer deposition (ALD) available in a common cleanroom to demonstrate large-area and flexible, high-performance NC FETs that operate stably in air over months.

RESULTS AND DISCUSSION

The experimental system in which we demonstrate this approach begins with approximately 4 nm diameter CdSe NCs, synthesized in organic solvents with bulky hydrocarbon surfactants serving as surface ligands. The surfactants are subsequently exchanged with a compact ligand, thiocyanate (SCN), and the NCs are dispersed in dimethylformamide and deposited by spin-coating to form 30−40 nm thick NC thin films, as described in our prior reports.[5,22] Previously, we demonstrated CdSe NC FETs employing gold-capped indium source and drain contacts. The devices were thermally annealed to 250 °C to (1) densify the film, in part, through decomposition of surface thiocyanates and (2) activate long-range indium diffusion from the electrodes and dope the film. In this design, the thin-film channels were characteristically glassy, NC solids with interparticle spacing varying from <0.5 nm to touching or near touching, and the electrodes constituted reservoirs of indium. These effects acted synergistically, giving rise to increased NC coupling and free carriers, respectively, with resultant FET electron mobilities as high as 27 cm^2/Vs.[5]

Here, we introduce the concept of using thermally activated indium diffusion to reverse air- and solvent-induced deterioration of CdSe NC FET performance. To separate the two effects of annealing, we first annealed the SCN-capped CdSe NC films in the absence of indium, densifying the film and decomposing the thiocyanate,[5,22] before thermally evaporating indium metal onto the film and reannealing to activate its diffusion into the film. FET characteristics of a device annealed in the absence of indium, with indium/gold electrodes subsequently deposited (Figure 1A, red), show low mobility (μ = 0.3 cm^2/Vs), low current modulation (I_{ON}/I_{OFF} = 10^4-10^5), high subthreshold swing (S = 18.3 V/dec), and severe hysteresis (ΔV_T = 17.4 V), which can be attributed in part to unpassivated NC surface states, especially after NC ligand exchange and decomposition with annealing. Devices were then reannealed to 250 °C with indium-containing electrodes, conditions which allow for long-range (~200 μm) indium diffusion into the film, as known for polycrystalline CdSe and as we reported for NC thin films.[5,23] These devices (Figure 1A, blue) have high-performance, characterized by dramatically higher μ = 16.4 cm^2/Vs and $I_{ON}/I_{OFF} > 10^7$, lower subthreshold swing (S = 3.2 V/dec), and reduced hysteresis (ΔV_T = 7.9 V). The device characteristics are dependent on the reannealing temperature between 150 and 250 °C, quantified by an increase in channel mobility and decrease in threshold voltage (Figure S1, Supporting Information). Wide-scan X-ray photoelectron spectroscopy

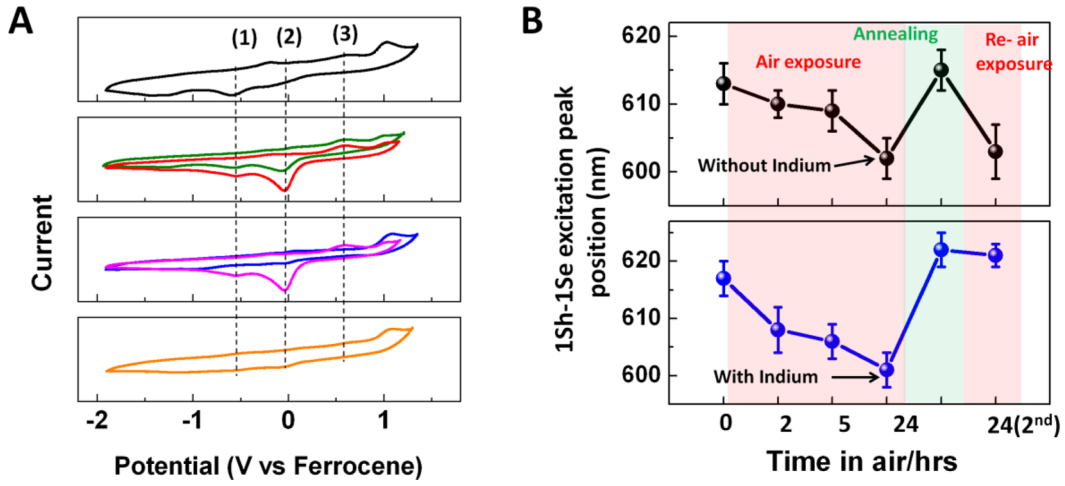

Figure 2. (A) Cyclic voltammograms of thiocyanate-exchanged CdSe NC thin films annealed at 250 °C for 10 min (black) and exposed to air for 1 h (green) and 24 h (red). Cyclic voltammograms of NC thin films exposed to air for 24 h and with 3 nm of deposited indium (blue) and without indium (magenta) annealed at 200 °C for 5 min. Cyclic voltammogram of the indium-diffused CdSe NC thin film after subsequent re-exposure to air for 24 h (orange). (B) $1S_{hole}-1S_{electron}$ peak position measured from diffuse reflectance spectra of thiocyanate-exchanged CdSe NC thin films annealed at 250 °C for 10 min as a function of air exposure over 24 h, upon annealing with 3 nm of deposited indium (blue) and without indium (black) at 200 °C for 5 min, and upon re-exposure to ambient air for 24 h.

of reference CdSe NC thin films with 3 nm of indium evaporated over the surface and subsequently annealed at 250 °C shows In $3d_{5/2}$ and $3d_{3/2}$ core levels at 444.48 and 452.18 eV, values identified previously with indium +3 ions,[24] which could be bound to the NC surface and/or incorporated into the CdSe NCs (Figure S2, Supporting Information).

It is well-known that, when semiconductor devices are exposed to air, their characteristics may be modified. Oxygen adsorbs to the surface of nanocrystalline (NCs and nanowires) and polycrystalline thin-film semiconductors, introducing new electronic states. In lead chalcogenides, oxygen creates low-lying acceptors, doping the semiconductor,[16,25−27] whereas in cadmium chalcogenides, deep-level acceptors are created, acting as electron traps that decrease the materials conductivity by 2−5 orders of magnitude.[28,29] Water adsorption on CdSe NCs has been reported to initially passivate and then oxidize the surface.[30,31] Water adsorption at the FET gate oxide interface has been shown to introduce electron traps in transistors composed of organic semiconductors,[32,33] ZnO,[34,35] Si,[36−38] and PbSe nanowires[39] and carbon nanotubes.[40,41] In our CdSe NC devices, the electron current deteriorates severely upon air exposure for 30 min (Figure 1A, green). However, upon reannealing at 200 °C for 5 min, the high-performance device characteristics are recovered (Figure 1A, black). As we present below, the recovery is consistent with a combination of desorption of surface oxygen and water[39] and passivation of surface defects through the activation of additional indium diffusion (Figure 1B).[5]

To understand the physical and chemical changes that accompany air exposure and annealing in the presence of indium, we performed cyclic voltammetry (CV) and UV−vis absorption measurements on annealed, CdSe NC thin-film samples before and after air exposure. Figure 2A shows the voltammogram recorded for an annealed sample (black). The oxidation (valence band) and reduction (conduction band) peaks are observed at 1.02 and −1.21 V, respectively, relative to the ferrocene/ferrocenium redox couple. The positions of midgap states in CdSe NC thin films also can be revealed in CV measurements: we observed additional peaks (1) and (3) between the conduction and valence edges in the voltammograms of annealed films that are not present as deposited (Figure S3, Supporting Information). States in this energy range have been assigned to Se and Cd vacancies at the NC surface, and we posit that thiocyanate decomposition to sulfur similarly introduces midgap states.[42−44] Upon exposing annealed CdSe NC films to air for 1 h (green) and 24 h (red), CV measurements show the growth of an additional reduction peak (2), which we ascribe to oxygen-related midgap states, following literature precedent.[42] However, those same 24 h air-exposed films, subsequently coated with indium and annealed (blue), showed dramatic reductions of the oxygen-related midgap states (2) and the other surface-related defects (1) and (3). More reactive indium metal is known to decrease chemisorbed oxygen in polycrystalline CdSe thin films.[45] In contrast, air-exposed films that were reannealed without indium showed no reduction in surface and oxygen-related defect states (magenta). To test the stability of the indium-diffused CdSe NC surface toward air oxidation, samples were re-exposed to air for an additional 24 h. The indium-passivated NC surface preserved a clean NC surface after further air exposure (orange), showing no observable reduction peak (2).

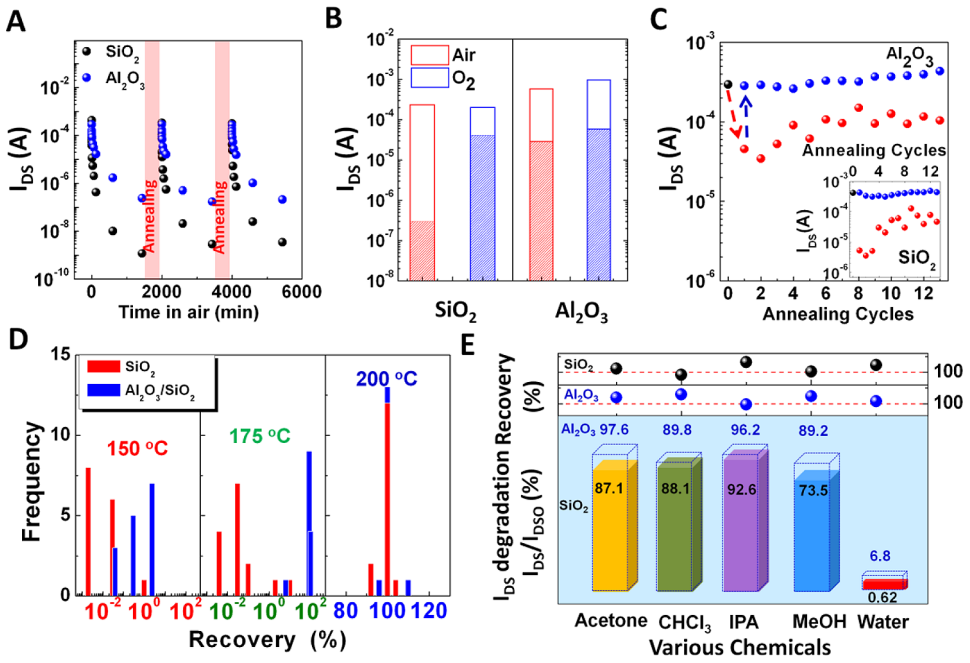

Figure 3. CdSe NC FET on-current (V_G = 50 V) in the linear regime (V_{DS} = 5 V) monitoring (A) cyclic degradation as a function of air-exposure time and recovery upon reannealing at 200 °C for 5 min, (B) degradation in air *versus* in pure oxygen environments (open bar, initial; filled bar, exposure), and (C) evolution in as-prepared FETs (black) upon successive cycles of air exposure for 30 min (red) and recovery by annealing at 200 °C for 5 min (blue). (D) Statistics in on-current recovery after 5 min of annealing at different temperatures. Note: Since all devices recover at an annealing temperature of 200 °C, the scale is narrowed. (E) NC FET degradation, characterized by the decrease in drain current I_{DS} (after exposure) to I_{DSO} (initial), upon immersion in acetone, chloroform, isopropyl alcohol, methanol, and water for 10 min at room temperature. Samples were dried using a nitrogen stream before electrical measurement. (Top) On-current recovery upon reannealing at 200 °C for 5 min after solvent immersion.

We characterized the absorbance spectra of films, exposed to air and annealed with and without indium, by diffuse reflectance and extracted the first absorption $1S_{electron}-1S_{hole}$ peak positions (Figure 2B and Figure S4, Supporting Information). For annealed CdSe NC samples exposed to air for 2, 5, and 24 h, the absorption spectra blue-shifted. The blue shift is consistent with oxidation of the NC surface, reducing the quantum confinement volume,[31,46] and oxygen and/or water adsorption, increasing the barrier height and/or width between NCs and leading to diminished NC−NC coupling.[29] Previous studies have reported surface oxygen and water desorption upon heating in vacuum or nitrogen and readsorption upon exposure to either gas or air, giving rise to reversible changes in semiconductor conductivity.[16,29,40,47] In our case, annealing the NC thin film in the nitrogen glovebox for 5 min at 200 °C red-shifted the absorption spectrum, returning it to its pre-exposure spectral characteristics, consistent with a similar desorption process (Figure 2B, black). Annealing a NC thin film with a 3 nm layer of deposited indium similarly reversed the influence of air exposure on the optical spectrum (Figure 2B, blue). NC films with and without indium upon annealing have nearly identical features characteristic of pre-exposed films, despite their significant differences by CV. We hypothesize that annealing desorbs weakly bound, physisorbed, and multilayer oxygen or water, which is detectable by UV−vis but not by CV, possibly due to displacement of these species by the acetonitrile solvent used in CV. In contrast, strongly chemisorbed surface oxygen is detected only by CV measurements (peak 2 in Figure 2). However, upon re-exposure of these NC films to air, the absorption of the indium-passivated NC film is stable, shifted by only 1 nm (blue), whereas without indium, a >10 nm blue shift was observed (black). The ability of indium to recover and passivate the film from gross electronic changes is seen in both optical and CV measurements.

We monitored the degradation in the drain current from the transfer characteristics in the linear regime (V_{DS} = 5 V) (Figure 3A) and in the saturation regime (V_{DS} = 50 V) (Figure S5, Supporting Information) as a function of air-exposure time before and after repeated recovery by annealing. Electrical measurements are more sensitive than optical and CV measurements to environmental influences. In the FET geometry, electrical measurements probe electron trapping both at the semiconductor NC surface and at the semiconductor−gate oxide interface due to oxygen and water adsorption. We investigated FETs with a commonly employed SiO_2 gate dielectric layer and an Al_2O_3/SiO_2 gate dielectric stack, which we previously showed reduced the interface trap density, improving CdSe NC FET performance.[5]

Upon air exposure, CdSe NC FETs with a SiO_2 gate dielectric layer rapidly degraded (with a time constant $\tau = 0.14$ min), whereas those fabricated with an Al_2O_3/SiO_2 gate dielectric stack degraded more slowly ($\tau = 5.00$ min) (Figure S6, Supporting Information), indicating the dominant role of semiconductor−dielectric interface trapping. To confirm the importance of both oxygen and water adsorption on the degradation of NC FETs, we compared NC FETs exposed side-by-side to air and to pure oxygen (Figure 3B). While the NC FET drain current is seen to degrade in pure oxygen, the drain current of NC FETs exposed to air degraded more and particularly dramatically for SiO_2 gate dielectric layers. Water is known to adsorb to surface hydroxyl groups on both SiO_2 and Al_2O_3 surfaces, but the larger concentration of surface hydroxyl *versus* bridged oxygen groups gives rise to the more acidic nature and greater water adsorption on SiO_2 in contrast to on more basic Al_2O_3.[48] Passivation of surface hydroxyl groups on SiO_2 gate dielectric layers with self-assembled silane monolayers substantially reduced device degradation (Figure S7, Supporting Information).

Annealing air-exposed CdSe NC devices, having both SiO_2 and Al_2O_3/SiO_2 gate dielectric layers, at 200 °C for 5 min under nitrogen restored the initial device characteristics, as shown in Figure 1. The device degradation and recovery can be repeatedly cycled many times upon air exposure and annealing. We hypothesize that annealing desorbs any oxygen and water (not detected by CV) bound to the NC surface, expels water residing at the gate oxide surface, and leads to additional diffusion of indium from the source and drain electrodes to recover the high-performance device characteristics. Time-of-flight secondary ion mass spectrometry (ToF-SIMS) analyses revealed a gradually increasing signal of indium ($^{113}In^+$) and a small, gradually increasing signal of the oxidized indium species (In_2O^+) as a function of an increasing number of annealing cycles, consistent with additional indium diffusion and surface indium gettering oxygen (Figure S8, Supporting Information).[45] We note that additional indium diffusion at 200 °C does not significantly dope CdSe NC thin films (Figure S1, Supporting Information), maintaining the low device off-currents. Devices with similar workfunction Al electrodes quickly degraded within 1 min of air exposure and did not show reversible behavior under the same annealing process (Figure S9, Supporting Information). Increasing the number of cycles of air exposure (for 30 min) and reannealing improves the air stability of the CdSe NC FETs, as measured in Figure 3C by the smaller drop in drain current in the linear regime ($V_{DS} = 5$ V) using both Al_2O_3/SiO_2 and (inset) SiO_2 gate dielectric layers (analogous behavior seen in the saturation regime is shown in Figure S10, Supporting Information). After repeated cycling through 13 times of air exposure and annealing, the device transfer characteristics did not show significant changes from the as-prepared, unexposed device behavior (Figure S11, Supporting Information). The devices with repeated cycling times of air exposure and annealing exhibit improved air stability consistent with greater indium passivation. Using indium as a recovery agent, integrated into the electrode architecture of the device, provides a powerful route to allow NC device fabrication in ambient air.

There is a critical range of annealing temperatures and times to recover the device characteristics that depends on the semiconductor−gate dielectric interface (Figure 3D). All devices showed recovered, high-performance behavior upon annealing at 200 °C for 5 min. For the devices with an Al_2O_3/SiO_2 gate dielectric stack, the recovery temperature can be lowered to 175 °C and 5 min. At lower temperatures of 150 °C, devices can be recovered by increasing the annealing time to 90 min (Figure S12A, Supporting Information). However, devices with a SiO_2 gate dielectric layer did not show as significant a recovery effect at temperatures <200 °C, requiring significantly longer times (6 h) to desorb surface-adsorbed water (Figure S12B, Supporting Information). It has been reported that 200 °C temperatures are required to eliminate water bound to silanols on SiO_2.[39,40,49]

We tested the electrical stability and recovery of indium-doped CdSe NC films after exposure to the solvents commonly used in standard photolithographic processing. Devices were dipped into each of the solvents; acetone, chloroform, isopropyl alcohol, methanol, and water; for 10 min at room temperature and then dried under a nitrogen flow before reprobing their FET characteristics. Figure 3E shows the percent degradation in drain current when the NC FETs, fabricated using both SiO_2 and Al_2O_3/SiO_2 gate dielectric layers, were exposed to various solvents. Exposure to acetone, chloroform, isopropyl alcohol, and methanol results in small reductions in the drain current, while substantial degradation in device performance is seen upon immersion in water, akin to the adverse effects of air exposure on device performance (Figure S13, Supporting Information). All of the devices, even devices that had dramatically deteriorated by water exposure, could be recovered upon reannealing.

We exploited the ability to recover the device performance after chemical and environmental exposure to fabricate wafer-scale integrated devices using photolithography and ALD encapsulation. Uniform CdSe NC thin films were deposited by spin-casting on 4 in. diameter Al_2O_3 (20 nm)/SiO_2(250 nm)/highly doped Si substrates, as shown in the inset of Figure 4A. Note here, an ultrathin (~1 nm), conformal, submonolayer of Al_2O_3 was deposited by ALD to prevent delamination of the NC thin film that was frequently observed without the ultrathin ALD oxide layer during subsequent photolithographic patterning (Figure S14, Supporting Information). While detailed studies of charge transport through NCs embedded in inorganic matrices remains to be explored, ALD oxides have been reported to offer significant

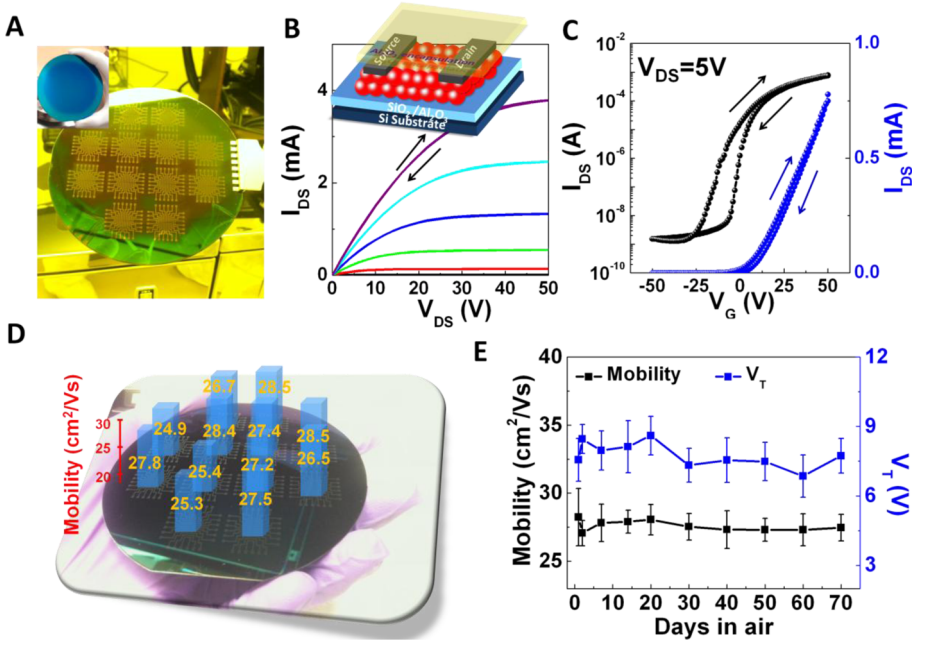

Figure 4. (A) Photograph of an array of 144 transistors fabricated by photolithographically patterning source and drain electrodes on [inset] a uniformly spin-cast CdSe NC thin film across a 4 in. Al_2O_3(20 nm)/SiO_2(250 nm)/highly doped Si wafer. (b) Output and (c) transfer characteristics (V_{DS} = 5 V) of NC FETs (channel length L = 30 μm, width W = 450 μm). [Inset] Schematic of the device structure. (d) Electron mobility of integrated CdSe NC devices over the large-area 4 in. substrate. (e) NC FET electron mobility (black) and threshold voltage (blue) as a function of time stored and operated in air.

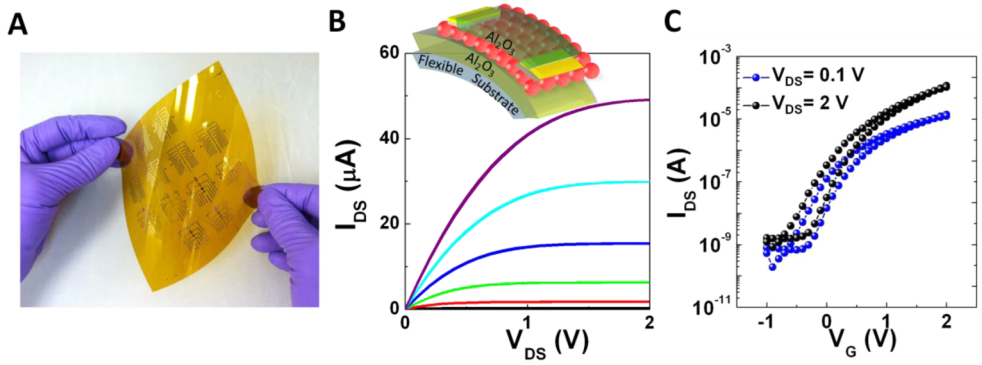

Figure 5. (A) Photograph of an array of photolithographically patterned NC FETs on a 4 in. square Kapton substrate. (b) Output and (c) transfer characteristics (V_{DS} = 0.1 and 2 V) of NC FETs (channel length L = 30 μm, width W = 450 μm). [Inset] Schematic of the NC FET structure.

potential in NC surface passivation.[50,51] A total of 144 sets of source and drain electrodes were defined using conventional photolithographic techniques to fabricate back-gate/top-contact FET arrays across the wafer (Figure 4A). The back-gate/top-contact configuration is desirable for high-performance devices, as we have previously reported that back-gate/bottom-contact geometry NC transistors display large contact resistance and therefore poor performance.[11] All 144 NC devices could be successfully recovered by reannealing. The recovered NC devices showed well-behaved, high-performance FET characteristics when operated in the nitrogen glovebox (Figure S15, Supporting Information). Further, by recognizing the recent progress using ALD oxide deposition on NC devices,[49,50] we employed a conventional ALD cleanroom tool to deposit a 50 nm Al_2O_3 encapsulation layer on NC devices. The temperatures (150 °C) commonly used in the ALD process make it possible to achieve *in situ* indium diffusion during the Al_2O_3 deposition, leading to fully passivated devices integrated in a single step.

Figure 4B, inset, shows a schematic of the photolithographically defined and ALD-encapsulated NC device configuration. Figure 4B,C presents typical output and transfer characteristics of these CdSe NC FETs. The devices show good linear and saturation characteristics. We compared the characteristics of devices with ALD passivation operating in ambient air to unencapsulated devices operating in ambient nitrogen (Figure S16, Supporting Information). The devices passivated with an Al_2O_3 layer exhibited lower off-current and hysteresis (ΔV_T = 2.8 V) than without the Al_2O_3

encapsulation (ΔV_T = 8.8 V), indicating that the encapsulation effectively prevented oxygen adsorption and repelled surface water. We characterized the statistics of device performance for FET arrays across large-area wafers, such as the example wafer shown in Figure 4D. All of the devices across the 4 in. wafer operated with a linear regime (V_{DS} = 5 V) μ = 26.9 ± 1.3 cm^2/Vs, high $I_{ON}/I_{OFF} > 10^6$, and a low subthreshold swing S = 2.9 ± 0.5 V/dec. In addition, in contrast to previous work, photolithography enabled the patterning of smaller channel lengths, readily to 2 μm, providing a route to study scaling in NC devices.

To test the air stability of devices, arrays of NC devices were stored and operated in air. Figure 4E demonstrates the carrier mobility and threshold voltage of NC FETs that were characterized over time. The NC device with an ALD encapsulation layer showed excellent operational stability with no decrease in performance over 70 days of measurement.

We further fabricated NC FETs on 4 in. flexible Kapton substrates (Figure 5A). The fabrication steps are described in ref 11, but here using the photolithography, ALD, and recovery processes described above. Figure 5B,C shows representative output and transfer characteristics of photolithographically defined, ALD-encapsulated, flexible NC FETs. The devices operate stably in ambient air at low voltages with a linear regime (V_{DS} = 0.1 V) μ = 21.4 cm^2/Vs and a saturation regime (V_{DS} = 2 V) μ = 20.8 cm^2/Vs. These NC FETs show high $I_{ON}/I_{OFF} > 10^5$, low subthreshold swing (S = 0.25 V/dec), low threshold voltage (V_T = 0.71 V), and low hysteresis (ΔV_T = 0.13 V) at V_{DS} = 0.1 V.

CONCLUSIONS

In conclusion, we introduced an *in situ* recovery agent, indium metal, that, upon thermal activation, reverses the detrimental effects of air and solvent exposure that degrade the electronic properties of high surface area semiconductor NC thin films and their devices. Employing a reservoir of indium metal in the electrodes of NC FETs, we exploited the recovery process to fabricate large-area and flexible, high-performance NC devices. The recovery process may be extended to other metal recovery agents and NC materials, opening up the wide range of conventional and unconventional semiconductor processes for low-cost, large-area fabrication of NC device technologies.

METHODS

Materials. Cadmium stearate was purchased from MP Biomedicals. Trioctylphosphine oxide (90%), octadecylamine (99%), selenium (99.99%, pellets), and tributylphosphine (97%) were purchased form Sigma-Aldrich. Ammonium thiocyanate was purchased from Acros and recrystallized with anhydrous alcohol.

NC Synthesis. CdSe NCs were synthesized following a modified literature procedure:[52] 20 g of trioctylphosphine oxide, 20 g of octadecylamine, and 2.10 g of cadmium stearate were held under vacuum for 1 h at 120 °C, then heated to 320 °C under nitrogen, then 10.0 mL of 1.25 M selenium in tributylphosphine solution was injected. Particle growth continued at 290 °C for 15 min. Synthesis was performed using standard air-free techniques, and purification by antisolvent precipitation was performed in a nitrogen glovebox with anhydrous solvents.

Ligand Exchange. Ligand exchange was performed in an inert nitrogen glovebox following our previously published procedure[5,11] and subsequently optimized for each batch of NCs. In a typical exchange, 1.0 mL of ammonium thiocyanate ranging in concentration from 100 to 250 mM in acetone was combined with 2.0 mL of CdSe NCs dispersed in hexane with an optical density ranging between 5 and 10 cm^{-1} at the first excitonic absorption feature (typically between 580 and 583 nm). The mixture was stirred with a vortexing mixer at 3000 rpm for 2 min, with complete precipitation of the NCs observed almost immediately. The subsequent slurry was centrifuged at 3000*g* for 1 min and then a clear, colorless supernatant discarded. The pellet was resuspended in 2.0 mL of tetrahydrofuran, the slurry mixed at 3000 rpm for 2 min, centrifuged at 3000*g* for 1 min, and then a clear, colorless supernatant was discarded. The pellet was resuspended in 2.0 mL of toluene, the slurry mixed at 3000 rpm for 1 min, centrifuged at 3000*g* for 1 min, and then a clear, colorless supernatant was discarded. Dimethylformamide was added to give the desired concentration, with gentle agitation applied to fully disperse the NCs.

CdSe NC Thin-Film Deposition. Ligand-exchanged CdSe NCs dispersed in dimethylformamide were spin-cast uniformally atop various substrates. A dispersion with an optical density of 40 was filtered through a 0.2 μm polytetrafluoroethylene filter and spin-cast at a rate of 500 rpm for 30 s, followed by 800 rpm for 30 s, yielding dense, crack-free uniform NC films.

FET Fabrication and Photolithographic Patterning. Device fabrication prior to photolithographic source and drain patterning followed previously published literature.[36] A 1 nm ultrathin layer of Al_2O_3 was grown on top of CdSe NC thin films by ALD (described below). Source and drain electrodes were patterned by standard photolithographic processes, forming top-contact bottom-gate FETs. For example, Microposit S1813 photoresist was spun at 4000 rpm for 25 s, followed by annealing at 115 °C for 60 s. Alignment was performed using a Nanonex NX-2600BA with an exposure energy of 90 mJ/cm^2. The exposed samples were soaked in Microposit MF-319 developer for 45 s to reveal the source and drain pattern. In/Au electrodes were thermally evaporated and later lifted-off in MicroChem Remover-PG.

Atomic Layer Deposition (ALD) Process. A Cambridge Nanotech Savannah 200 ALD system was used to grow Al_2O_3 from trimethylaluminum and water precursors. For both ultrathin 1 nm oxide layers, used to prevent NC thin-film delamination, and ~50 nm thick encapsulation layers, the deposition was carried out at a processing temperature of 150 °C.

Field-Effect Transistor (FET) Characterization. FET device characterization was collected using Karl Suss PM5 probe stations, one mounted in a nitrogen-filled glovebox and another in ambient air, and connected to an Agilent 4156C semiconductor parameter analyzer.

Cyclic Voltammetric (CV) Characterization. CV measurements were conducted using an Epsilon electrochemical workstation, with the C3 cell stand mounted in the nitrogen glovebox. The three-electrode system was set up in an organic electrolyte of 0.01 M of $TBAHF_6$ in acetonitrile. Then, 40 nm CdSe NC thin films were deposited on top of Pd-coated Si substrates that served as the working electrode. A Pt wire and Ag in 0.01 M of $AgNO_3$ (nonaqueous) in $TBAHF_6$/acetonitrile functioned as the counter and reference electrodes, respectively. CV scans were obtained at a scan rate of 20 mV/s between −1.8 and 1.8 V relative to the Ag/Ag^+ electrode. All the potentials were scaled relative to reference measurements of the redox couple ferrocene/ferrocenium.

UV−Visible Absorption Spectroscopy. Spectra of NC thin films on glass substrates were taken in diffuse reflectance mode on a Cary 5000 spectrophotometer (formerly Varian Inc., now Agilent Technologies) at 2 nm spectral bandwidth, using an integrating

sphere accessory (Praying Mantis, Harrick Scientific). NC thin-film samples were removed from the nitrogen glovebox just prior to measurement to limit air exposure to 3−4 min. To determine the energy of the $1S_{hole}-1S_{electron}$ transition, analytic second derivatives were calculated from the spectra, and the absorption maximum was determined from the negative extremum of the second derivative.

Time-of-Flight Secondary Ion Mass Spectrometry (ToF-SIMS). ToF-SIMS experiments were performed using an ION-TOF TOF.SIMS 4 (IONTOF GmbH, Münster, Germany) equipped with a 25 keV Bi^{3+} ion source for spectral acquisition and 8 keV SF^{5+} ion source for sputtering. Both beams hit the target at an angle of 45°. The ion dose densities were 5×10^9 and 1.8×10^{13} ions/cm^2 per cycle, respectively. A low-energy electron flood gun was used for charge compensation. Lateral profiling of the $^{113}In^+$ and In_2O^+ distributions was characterized in the NC channel between the In/Au source and drain electrodes.

Conflict of Interest: The authors declare no competing financial interest.

Acknowledgment. We thank S. Muramoto and J.G. Gillen for XPS and SIMS measurements. Cyclic voltammetry, the time- and temperature-dependent degradation and recovery of device performance with air, oxygen, and solvent exposure, and the fabrication and characterization of ALD-encapsulated, air-stable NC devices were supported by the NSF MRSEC under Award No. DMR11-20901. The synthesis of CdSe NCs, the development of the ultrathin ALD oxide, the photolithographic patterning of FETs, and the fabrication and characterization of flexible FETs were supported by the U.S. Department of Energy Office of Basic Energy Sciences, Division of Materials Science and Engineering, under Award No. DE-SC0002158. CdSe NC ligand exchange and thin-film deposition was supported by NSF-CBET, Grant CBET-0854226. Absorption measurements were supported by the NSF Solar Program under Award No. DMS-0935165. B.T.D. acknowledges support by the IBM Graduate Fellowship. C.B.M. is grateful for the support of the Richard Perry University Professorship.

Supporting Information Available: Experimental details and supplementary figures as described in the text. This material is available free of charge *via* the Internet at http://pubs.acs.org.

REFERENCES AND NOTES

1. Alivisatos, A. P. Semiconductor Clusters, Nanocrystals, and Quantum Dots. *Science* **1996**, *271*, 933–937.
2. Murray, C. B.; Kagan, C. R.; Bawendi, M. G. Synthesis and Characterization of Monodisperse Nanocrystals and Close-Packed Nanocrystal Assemblies. *Annu. Rev. Mater. Sci.* **2000**, *30*, 545–610.
3. Talapin, D. V.; Murray, C. B. PbSe Nanocrystal Solids for n- and p-Channel Thin Film Field-Effect Transistors. *Science* **2005**, *310*, 86–89.
4. Lee, J.-S.; Kovalenko, M. V.; Huang, J.; Chung, D. S.; Talapin, D. V. Band-like Transport, High Electron Mobility and High Photoconductivity in All-Inorganic Nanocrystal Arrays. *Nat. Nanotechnol.* **2011**, *6*, 348–352.
5. Choi, J.-H.; Fafarman, A. T.; Oh, S. J.; Ko, D.-K.; Kim, D. K.; Diroll, B. T.; Muramoto, S.; Gillen, J. G.; Murray, C. B.; Kagan, C. R. Bandlike Transport in Strongly Coupled and Doped Quantum Dot Solids: A Route to High-Performance Thin-Film Electronics. *Nano Lett.* **2012**, *12*, 2631–2638.
6. Chung, D. S.; Lee, J.-S.; Huang, J.; Nag, A.; Ithurria, S.; Talapin, D. V. Low Voltage, Hysteresis Free, and High Mobility Transistors from All-Inorganic Colloidal Nanocrystals. *Nano Lett.* **2012**, *12*, 1813–1820.
7. Semonin, O. E.; Luther, J. M.; Choi, S.; Chen, H.-Y.; Gao, J.; Nozik, A. J.; Beard, M. C. Peak External Photocurrent Quantum Efficiency Exceeding 100% *via* MEG in a Quantum Dot Solar Cell. *Science* **2011**, *334*, 1530–1533.
8. Sargent, E. H. Colloidal Quantum Dot Solar Cells. *Nat. Photonics* **2012**, *6*, 133–135.
9. Coe, S.; Woo, W.-K.; Bawendi, M.; Bulović, V. Electroluminescence from Single Monolayers of Nanocrystals in Molecular Organic Devices. *Nature* **2002**, *420*, 800–803.
10. Caruge, J. M.; Halpert, J. E.; Wood, V.; Bulović, V.; Bawendi, M. G. Colloidal Quantum-Dot Light-Emitting Diodes with Metal-Oxide Charge Transport Layers. *Nat. Photonics* **2008**, *2*, 247–250.
11. Kim, D. K.; Lai, Y.; Diroll, B. T.; Murray, C. B.; Kagan, C. R. Flexible and Low-Voltage Integrated Circuits Constructed from High-Performance Nanocrystal Transistors. *Nat. Commun.* **2012**, *3*, 1216.
12. Liu, W.; Lee, J.-S.; Talapin, D. V. III−V Nanocrystals Capped with Molecular Metal Chalcogenide Ligands: High Electron Mobility and Ambipolar Photoresponse. *J. Am. Chem. Soc.* **2013**, *135*, 1349–1357.
13. Ip, A. H.; Thon, S. M.; Hoogland, S.; Voznyy, O.; Zhitomirsky, D.; Debnath, R.; Levina, L.; Rollny, L. R.; Carey, G. H.; Fischer, A.; *et al.* Hybrid Passivated Colloidal Quantum Dot Solids. *Nat. Nanotechnol.* **2012**, *7*, 577–582.
14. Cho, K.-S.; Lee, E. K.; Joo, W. J.; Jang, E.; Kim, T. H.; Lee, S. J.; Kwon, S.-J.; Han, J. Y.; Kim, B.-K.; Choi, B. L.; *et al.* High-Performance Crosslinked Colloidal Quantum-Dot Light-Emitting Diodes. *Nat. Photonics* **2009**, *3*, 341–345.
15. Sun, L.; Choi, J. J.; Stachnik, D.; Bartnik, A. C.; Hyun, B. R.; Malliaras, G. G.; Hanrath, T.; Wise, F. W. Bright Infrared Quantum-Dot Light-Emitting Diodes through Inter-dot Spacing Control. *Nat. Nanotechnol.* **2012**, *7*, 369–373.
16. Leschkies, K. S.; Kang, M. S.; Aydil, E. S.; Norris, D. J. Influence of Atmospheric Gases on the Electrical Properties of PbSe Quantum-Dot Films. *J. Phys. Chem. C* **2010**, *114*, 9988–9996.
17. Luther, J. M.; Law, M.; Beard, M. C.; Song, Q.; Reese, M. O.; Ellingson, R. J.; Nozik, A. J. Schottky Solar Cells Based on Colloidal Nanocrystal Films. *Nano Lett.* **2008**, *8*, 3488–3492.
18. Koleilat, G. I.; Levina, L.; Shukla, H.; Myrskog, S. H.; Hinds, S.; Pattantyus-Abraham, A. G.; Sargent, E. H. Efficient, Stable Infrared Photovoltaics Based on Solution-Cast Colloidal Quantum Dots. *ACS Nano* **2008**, *2*, 833–840.
19. Oh, S. J.; Berry, N. E.; Choi, J.-H.; Gaulding, E. A.; Paik, T.; Hong, S.-H.; Murray, C. B.; Kagan, C. R. Stoichiometric Control of Lead Chalcogenide Nanocrystal Solids To Enhance Their Electronic and Optoelectronic Device Performance. *ACS Nano* **2013**, *7*, 2413–2421.
20. Zarghami, M. H.; Liu, Y.; Gibbs, M.; Gebremichael, E.; Webster, C.; Law, M. p-Type PbSe and PbS Quantum Dot Solids Prepared with Short-Chain Acids and Diacids. *ACS Nano* **2010**, *4*, 2475–2485.
21. Kang, M. S.; Lee, J.; Norris, D. J.; Frisbie, C. D. High Carrier Densities Achieved at Low Voltages in Ambipolar PbSe Nanocrystal Thin-Film Transistors. *Nano Lett.* **2009**, *9*, 3848–3852.
22. Fafarman, A. T.; Koh, W.-k.; Diroll, B. T.; Kim, D. K.; Ko, D.-K.; Oh, S. J.; Ye, X.; Doan-Nguyen, V.; Crump, M. R.; Reifsnyder, D. C.; *et al.* Thiocyanate-Capped Nanocrystal Colloids: Vibrational Reporter of Surface Chemistry and Solution-Based Route to Enhanced Coupling in Nanocrystal Solids. *J. Am. Chem. Soc.* **2011**, *133*, 15753–15761.
23. Scilla, G. J.; Luo, F. C. Indium Diffusion in Cadmium Selenide Thin Film Transistors with Indium-Gold Contacts. *Appl. Phys. Lett.* **1983**, *42*, 538–540.
24. He, Z.; Jie, J.; Zhang, W.; Zhang, W.; Luo, L.; Fan, X.; Yuan, G.; Bello, I.; Lee, S.-T. Tuning Electrical and Photoelectrical Properties of CdSe Nanowires *via* Indium Doping. *Small* **2009**, *5*, 345–350.
25. Kim, D. K.; Vemulkar, T. R.; Oh, S. J.; Koh, W.-k.; Murray, C. B.; Kagan, C. R. Ambipolar and Unipolar PbSe Nanowire Field-Effect Transistors. *ACS Nano* **2011**, *5*, 3230–3236.
26. Oh, S. J.; Kim, D. K.; Kagan, C. R. Remote Doping and Schottky Barrier Formation in Strongly Quantum Confined Single PbSe Nanowire Field-Effect Transistors. *ACS Nano* **2012**, *6*, 4328–4334.
27. Harada, R. H.; Minden, H. T. Photosensitization of PbS Films. *Phys. Rev.* **1956**, *102*, 1258–1262.
28. Samanta, D.; Samanta, B.; Chaudhuri, A. K.; Ghorai, S.; Pal, U. Electrical Characterization of Stable Air-Oxidized CdSe Films Prepared by Thermal Evaporation. *Semicond. Sci. Technol.* **1996**, *11*, 548–553.

29. Wu, C.-h.; Bube, R. H. Thermoelectric and Photothermoelectric Effects in Semiconductors: Cadmium Sulfide Films. *J. Appl. Phys.* **1974**, *45*, 648–660.
30. Cahen, D.; Hodes, G. Molecules and Electronic Materials. *Adv. Mater.* **2002**, *14*, 789–798.
31. Cordero, S. R.; Carson, P. J.; Estabrook, R. A.; Strouse, G. F.; Buratto, S. K. Photo-Activated Luminescence of CdSe Quantum Dot Monolayers. *J. Phys. Chem. B* **2000**, *104*, 12137–12142.
32. Egginger, M.; Bauer, S.; Schwödiauer, R.; Neugebauer, H.; Sariciftci, N. S. Current *versus* Gate Voltage Hysteresis in Organic Field Effect Transistors. *Monatsh. Chem.* **2009**, *140*, 735–750.
33. Gu, G.; Kane, M. G. Moisture Induced Electron Traps and Hysteresis in Pentacene-Based Organic Thin-Film Transistors. *Appl. Phys. Lett.* **2008**, *92*, 053305.
34. Goldberger, J.; Sirbuly, D. J.; Law, M.; Yang, P. ZnO Nanowire Transistors. *J. Phys. Chem. B* **2005**, *109*, 9–14.
35. Choi, J.-H.; Khang, D.-Y.; Myoung, J.-M. Fabrication and Characterization of ZnO Nanowire Transistors with Organic Polymer as a Dielectric Layer. *Solid State Commun.* **2008**, *148*, 126–130.
36. Wang, D.; Sheriff, B. A.; Heath, J. R. Silicon p-FETs from Ultrahigh Density Nanowire Arrays. *Nano Lett.* **2006**, *6*, 1096–1100.
37. Paska, Y.; Stelzner, T.; Christiansen, S.; Haick, H. Enhanced Sensing of Nonpolar Volatile Organic Compounds by Silicon Nanowire Field Effect Transistors. *ACS Nano* **2011**, *5*, 5620–5626.
38. Choi, J.-H.; Sung, J.; Moon, K.-J.; Jeon, J.; Kang, Y. H.; Lee, T. I.; Park, C.; Myoung, J.-M. Intrinsic Memory Behavior of Rough Silicon Nanowires and Enhancement *via* Facile Ag NPs Decoration. *J. Mater. Chem.* **2011**, *21*, 13256–13261.
39. Kim, D. K.; Lai, Y.; Vemulkar, T. R.; Kagan, C. R. Flexible, Low Voltage and Low Hysteresis PbSe Nanowire Field-Effect Transistors. *ACS Nano* **2011**, *5*, 10074–10083.
40. Kim, W.; Javey, A.; Vermesh, O.; Wang, Q.; Li, Y.; Dai, H. Hysteresis Caused by Water Molecules in Carbon Nanotube Field-Effect Transistors. *Nano Lett.* **2003**, *3*, 193–198.
41. Aguirre, C. M.; Levesque, P. L.; Paillet, M.; Lapointe, F.; St-Antoine, B. C.; Desjardins, P.; Martel, R. The Role of the Oxygen/Water Redox Couple in Suppressing Electron Conduction in Field-Effect Transistors. *Adv. Mater.* **2009**, *21*, 3087–3091.
42. Kuçur, E.; Bücking, W.; Giernoth, R.; Nann, T. Determination of Defect States in Semiconductor Nanocrystals by Cyclic Voltammetry. *J. Phys. Chem. B* **2005**, *109*, 20355–20360.
43. Poles, E.; Selmarten, D. C.; Mićić, O. I.; Nozik, A. J. Anti-Stokes Photoluminescence in Colloidal Semiconductor Quantum Dots. *Appl. Phys. Lett.* **1999**, *75*, 971–973.
44. Hoffmann, H. J.; Huber, E. Generation-Recombination Noise and Defect Levels in Semiconducting CdSe Crystals. *Physica B+C* **1981**, *111*, 249–256.
45. De Baets, J.; Van Calster, A.; De cubber, A.-M.; De Smet, H.; Vanfleteren, J. Modelling Poly-CdSe TFTs for AMLCD. *Proc. – Electrochem. Soc.* **1995**, *94–35*, 228–231.
46. Nirmal, M.; Dabbousi, B.; Bawendi, M. G.; Macklin, J. J.; Trautman, J. K.; Harris, T. D.; Brus, L. E. Fluorescence Intermittency in Single Cadmium Selenide Nanocrystals. *Nature* **1996**, *383*, 802–804.
47. Shear, H.; Hilton, E. A.; Bube, R. H. Oxygen Chemisorption Effects on Photoconductivity in Sintered Layers. *J. Electrochem. Soc.* **1965**, *112*, 997–1002.
48. Arico, A. S.; Baglio, V.; Di Blasi, A.; Creti, P.; Antonucci, P. L.; Antonucci, V. Influence of the Acid–Base Characteristics of Inorganic Fillers on the High Temperature Performance of Composite Membranes in Direct Methanol Fuel Cells. *Solid State Ionics* **2003**, *161*, 251–265.
49. Zhuravlev, L. T. The Surface Chemistry of Amorphous Silica. Zhuravlev Model. *Colloids Surf., A* **2000**, *173*, 1–38.
50. Liu, Y.; Gibbs, M.; Perkins, C. L.; Tolentino, J.; Zarghami, M. H.; Bustamante, J.; Law, M. Robust, Functional Nanocrystal Solids by Infilling with Atomic Layer Deposition. *Nano Lett.* **2011**, *11*, 5349–5355.
51. Liu, Y.; Tolentino, J.; Gibbs, M.; Ihly, R.; Perkins, C. L.; Liu, Y.; Crawford, N.; Hemminger, J. C.; Law, M. PbSe Quantum Dot Field-Effect Transistors with Air-Stable Electron Mobilities above 7 $cm^2 V^{-1} s^{-1}$. *Nano Lett.* **2013**, *13*, 1578–1587.
52. Qu, L.; Peng, X. Control of Photoluminescence Properties of CdSe Nanocrystals in Growth. *J. Am. Chem. Soc.* **2002**, *124*, 2049–2055.